

导波模式对锥形半导体激光器输出特性的影响

袁庆贺^{2,3}, 井红旗^{2*}, 刘素平², 马骁宇^{2,3}, 马晓辉¹

¹ 长春理工大学高功率半导体激光国防科技重点实验室, 吉林 长春 130022;

² 中国科学院半导体研究所光电子器件国家工程研究中心, 北京 100083;

³ 中国科学院大学材料科学与光电技术学院, 北京 100049

摘要 近年来,锥形半导体激光器的发展受到越来越多的关注,这主要是因为它能够提供高功率高光束质量的激光输出,但过高的输出功率会导致光束质量的迅速恶化。利用专业光波导仿真软件 Rsoft,对比分析了增益波导结构和折射率波导结构对锥形半导体激光器输出特性的影响,主要研究了不同导波模式下的近/远场分布以及功率-电流-电压特性。结果表明,在相同电压条件下,相较于折射率波导结构,具有增益波导结构的锥形激光器的输出功率虽相对较低,但其出光面上的光场分布更均匀,可以有效降低空间烧孔效应的影响,且其远场分布也较均匀。研究结论为锥形半导体激光器的结构设计提供了参考。

关键词 激光器; 锥形激光器; 增益波导; 折射率波导; Rsoft; 仿真

中图分类号 TN248.4

文献标志码 A

doi: 10.3788/CJL202148.0901001

1 引言

大功率半导体激光器具有体积小、质量轻、结构简单、能量密度高等优点。大功率半导体激光器现已广泛应用于工业生产、激光通信、激光医疗、激光显示以及国防等方面^[1-6]。随着应用领域的不断拓展,人们对半导体激光器的性能也提出了更高的要求。为了提高半导体激光器的输出功率和光束质量,研究人员提出了锥形激光器的设计思路。

锥形半导体激光器一般由脊型波导构成的单模区和锥形放大区两部分组成。脊型波导构成的单模区起模式过滤的作用,保证器件基模振荡;锥形放大区起功率放大作用,同时可以减小输出腔面的功率密度、抑制出光面灾变性光学损伤。德国 FBH 研究所一直致力于高光束质量锥形半导体激光器的研究,先后报道过多种波长的近衍射极限大功率器件。808 nm 波长器件在 4.4 W 功率输出时,可得 1.9 的光束质量因子^[7]; 979 nm 器件最高输出功率为 12 W,在 11.4 W 功率输出时,光束质量因子仅为

1.1^[8]。Müller 等^[9]采用非对称超大光腔的外延设计,研制了 1030 nm 含有布拉格反射器(DBR)的锥形激光器,在 15 °C 时实现了 8.1 W 的主瓣功率,光束质量因子为 1.1。2017 年,该团队通过在脊型波导区两侧进行离子注入,增强了脊型区的模式选择作用,并进一步优化前后腔面的反射率,15 °C 时实现了 9.1 W 的主瓣功率,光束质量因子为 1.2^[10]。

锥形半导体激光器虽然能够输出高功率高光束质量的激光,但与大功率宽条型半导体激光器一样,高功率输出时光束不稳定,光束容易发生扭曲,进而引起丝状(Filamentation)发光现象。产生上述现象的原因主要有两个:一是脊型波导构成的单模区的模式过滤作用不理想,注入到锥形区的光束并非基模;二是在锥形放大区,热诱导或空间烧孔等原因引起折射率变化,导致光束自聚焦。本文采用专业光波导仿真软件 Rsoft,对比分析了增益波导结构和折射率波导结构对锥形激光器单模区模式过滤作用的影响,以及激光器输出特性的差异,以期高功率高光束质量锥形半导体激光器的设计提供参考。

收稿日期: 2020-09-25; 修回日期: 2020-10-16; 录用日期: 2020-11-04

基金项目: 国防科技重点基金(6142405041803)

*E-mail: jinghq@semi.ac.cn

2 理论基础

2.1 模拟计算的相关理论

半导体激光器是建立在光沿着光波导传播的基础之上的,为了对其进行设计和优化,需要通过光波传播技术来精确模拟光在非均匀光学结构中的传播。目前已有一系列光波传播技术。本文通过求解波动方程,计算给定边界条件下计算域内的电磁场分布。

在标量场假设(即忽略极化的影响且光束传播被限制在狭窄的角度范围内)条件下,可以将波动方程写成单色波的 Helmholtz 方程形式^[11-12]:

$$\frac{\partial^2 \psi}{\partial x^2} + \frac{\partial^2 \psi}{\partial y^2} + \frac{\partial^2 \psi}{\partial z^2} + k_1^2(x, y, z)\psi = 0, \quad (1)$$

式中: ψ 为场; (x, y, z) 为点坐标; $k_1(x, y, z) = k_0 n(x, y, z)$, k_0 为自由空间波数, $k_0 = 2\pi/\lambda$, λ 为传输光波长, $n(x, y, z)$ 为折射率。此处,标量电场可以写成 $E(x, y, z, t) = \psi(x, y, z) \exp(-i\omega t)$, 其中 t 为时间, ω 为频率。(1)式就完全由折射率 $n(x, y, z)$ 决定。

考虑到在典型的光导波问题中,磁场中变化最快的是沿波导轴方向(一般是 z 轴方向)传播的相位变化。通过引入缓慢变化的磁场 $u(x, y, z)$, 可以将这种快速变化排除在问题之外:

$$\psi(x, y, z) = u(x, y, z) \exp(i\bar{k}z), \quad (2)$$

式中: z 为 z 轴方向的坐标值; \bar{k} 为常数,表征场 ψ 的平均相位变化,被称为参考波数。参考波数通常用参考折射率 \bar{n} 表示,即 $\bar{k} = k_0 \bar{n}$, 代入 Helmholtz 方程可得

$$\frac{\partial^2 u}{\partial z^2} + 2i\bar{k} \frac{\partial u}{\partial z} + \frac{\partial^2 u}{\partial x^2} + \frac{\partial^2 u}{\partial y^2} + (k_1^2 - \bar{k}^2)u = 0. \quad (3)$$

(3)式完全等同于精确的亥姆霍兹方程。假设 $u(x, y, z)$ 在 z 方向上的变化足够慢,可以忽略(3)式中的第一项,即缓变包络近似,从而(3)式可以写成

$$\frac{\partial u}{\partial z} = \frac{i}{2\bar{k}} \times \frac{\partial^2 u}{\partial x^2} + \frac{\partial^2 u}{\partial y^2} + (k_1^2 - \bar{k}^2)u. \quad (4)$$

因此可以得出传播场 $E(x, y, z)$ 为

$$E(x, y, z) = u(x, y, z) \exp(i\bar{k}z). \quad (5)$$

(5)式中的 \bar{k} 是与材料的折射率相关的,而材料折射率的分布又取决于载流子浓度和温度的分布。利用泊松方程自洽求解电子和空穴的电流连续性方程,可以确定半导体激光器内的载流子浓度。

在量子阱中,束缚态连续性方程^[13]为

$$q \frac{\partial n_{e/h}^{2D}}{\partial t} = \pm Q_{e/h,||} - qR^{\text{dark}} - qR^{\text{stim}} - qR^{\text{spon,bond}} + qR_{e/h}^{\text{capture}}, \quad (6)$$

连续态连续性方程^[13]为

$$q \frac{\partial n_{e/h}^{3D}}{\partial t} = \pm Q_{e/h} - qR^{\text{dark}} - qR^{\text{stim}} - qR^{\text{spon,bulk}} - qR_{e/h}^{\text{capture}}, \quad (7)$$

泊松方程^[13]为

$$\nabla \varepsilon \nabla \varphi + q(N_D^+ - N_A^- + p - n) = 0, \quad (8)$$

式中: $n_{e/h}^{2D}$ 和 $n_{e/h}^{3D}$ 分别为束缚态和连续态的载流子浓度; $Q_{e/h,||}$ 和 $Q_{e/h}$ 分别为外加电流提供的量子阱平面和激光器芯片表面的载流子通量,对于束缚态,只需考虑量子阱平面内的载流子通量,因为生长方向上的载流子分布是由限制势内的波函数决定的; q 为电荷电量; R^{dark} 为非辐射复合速率; R^{stim} 为受激发射速率; $R^{\text{spon,bulk}}$ 和 $R^{\text{spon,bond}}$ 分别为体/连续介质和束缚载流子的自发复合速率; $R_{e/h}^{\text{capture}}$ 为电子和空穴的俘获速率; φ 为电势; N_D^+ 和 N_A^- 分别为施主和受主杂质的电离浓度; n 和 p 分别为电子和空穴的浓度; ε 为介电常数。

半导体激光器中温度的分布可以利用热传导方程进行求解,其具体形式^[14]为

$$\nabla(-k \nabla T) = W, \quad (9)$$

式中: k 为热导率; W 为热产生率。温度的变化会引起材料折射率发生变化,Wenzel 等^[15]证实了折射率的实部与载流子密度的平方根呈正比。本文在进行计算时也考虑了折射率与温度的依赖关系。

折射率是温度和载流子浓度的函数,而温度和载流子浓度的分布又取决于光场强度和注入电流,因此(4)、(6)、(7)、(8)、(9)式之间形成了一个耦合的非线性系统。通过迭代求解,可以得出半导体激光器中场的分布情况。

2.2 器件结构设计的相关理论

对于锥形半导体激光器,器件结构的设计至关重要,其直接关系到激光器性能的好坏。

根据等效折射率方法,计算折射率波导结构的一阶模截止条件。将单模区和两侧刻蚀区简化为对称的三层平板实折射率波导,其一阶模截止的宽度^[16]为

$$\omega_1 = \frac{\lambda}{2\sqrt{N_{\text{eff1}}^2 - N_{\text{eff2}}^2}}, \quad (10)$$

式中: N_{eff1} 和 N_{eff2} 分别为单模区和单模区两侧的有效模式折射率; ω_1 为单模区的宽度。

单模区的长度对锥形半导体激光器的光束质量有重要影响。如果单模区的长度过短,模式过滤会不充分,随着单模区长度的增加,模式得到有效过滤,光束稳定。如果单模区的长度过长,过高的能量注入到锥形区,容易发生自聚焦和光束扭曲,引起光束质量恶化。因此,单模区的长度应进行优化设计。

在锥形激光器的设计中,一个重要的参数就是锥形角度。为了保证从单模区进入锥形区的光束的低损耗传输,避免光束传播过程中基模能量耦合进高阶模或辐射模,锥形角度应小于基模衍射角。基模衍射角 $\theta^{[17]}$ 定义为

$$\theta = \frac{\lambda}{n\tau w_1} \left[2\arctan\left(\frac{b}{1-b}\right)^{1/2} \times \frac{1}{\pi} \right], \quad (11)$$

$$b = \frac{N_{\text{neff}-\infty}^2 - n^2}{N_{\text{neff}}^2 - n^2}, \quad (12)$$

式中: $N_{\text{neff}-\infty}$ 为单模区宽度 τw_1 趋于无穷大时的有效折射率。对于不同的器件,基模衍射角一般为 $6^\circ \sim 7^\circ$ 。

锥形区作为锥形激光器的功率放大部分,对单模区输入的基模光束进行光放大。通常情况下,较长的锥形区可以降低光功率密度,从而提高输出功率和光束质量,但是过长的腔长会使激光器阈值电流上升,效率降低,因此锥形区的长度要综合考量^[18]。

3 结果分析与讨论

图 1(a)、(b)分别为增益波导结构和折射率波

表 1 结构的相关参数

Table 1 Related parameters of structure

Waveguide type	Size of single mode area / ($\mu\text{m} \times \mu\text{m}$)	Taper length / μm	Width of output facet / μm	Etching depth / μm	Taper angle / ($^\circ$)
Gain waveguide	800×3	1200	60	0	3
Refractive index waveguide	800×3	1200	60	0.5	3

3.1 近场特性

近场通常是指半导体激光器前腔面上的光场分布。为了更好分析不同导波模式下单模区对前腔面反射光的过滤作用,同时也给出了后腔面上光场的分布情况。

图 2 给出的是 1.55 V 电压条件下,两种导波模式后腔面的向前传播光场分布,其中 X、Y 分别为激光器芯片后腔面的宽度和厚度。图 2(a)、(b)分别为增益波导结构激光器后腔面的前向光场及其对应的强度分布情况,图 2(c)、(d)分别为折射率波导结构激光器后腔面的前向光场及其对应的强度分布。可以看出,增益波导结构激光器后腔面的光场分布

导结构锥形半导体激光器的结构示意图。增益波导结构在平行于 PN 结平面方向上没有引入任何折射率差,利用限定注入电流的区域形成波导,并限制侧向模式,如质子轰击条型激光器。折射率波导结构是利用有源区厚度的变化或有源区与无源区之间的损耗差,形成侧向有效折射率差,从而形成内建的折射率波导,如脊型结构。

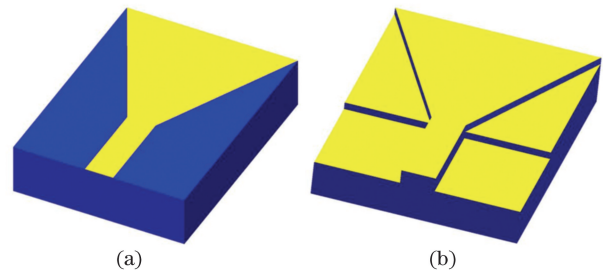


图 1 锥形半导体激光器的结构示意图。(a)增益波导;
(b)折射率波导

Fig. 1 Structural diagrams of tapered semiconductor laser.

(a) Gain waveguide; (b) refractive index waveguide

为了研究导波模式对锥形半导体激光器的影响,分别对增益波导结构和折射率波导结构激光器进行模拟,相关参数如表 1 所示。除了折射率波导结构激光器的脊型波导刻蚀深度为 $0.5 \mu\text{m}$ 外,其余相关参数完全一致。激光器传输光波长为 980 nm ,前腔面(即出光面)和后腔面的反射率分别为 1% 和 99%。

比较平滑,没有较高的尖峰出现,而折射率波导结构激光器后腔面的光场分布则相对比较粗糙,有众多小的尖峰出现,且在单模区两侧光场强度较强。这主要是因为折射率波导结构对光的限制作用较强,前腔面反射回来的光很大一部分被限制在单模区及其两侧,导致单模区模态过滤效果降低。

图 3 显示的是 1.55 V 电压条件下出光面上的光场分布情况,其中 X'、Y' 分别为激光器芯片前腔面的宽度和厚度。图 3(a)、(b)为增益波导结构激光器前腔面的光场及其对应的强度分布情况,图 3(c)、(d)为折射率波导结构激光器前腔面的光场及其对应的强度分布。可以看出,增益波导结构

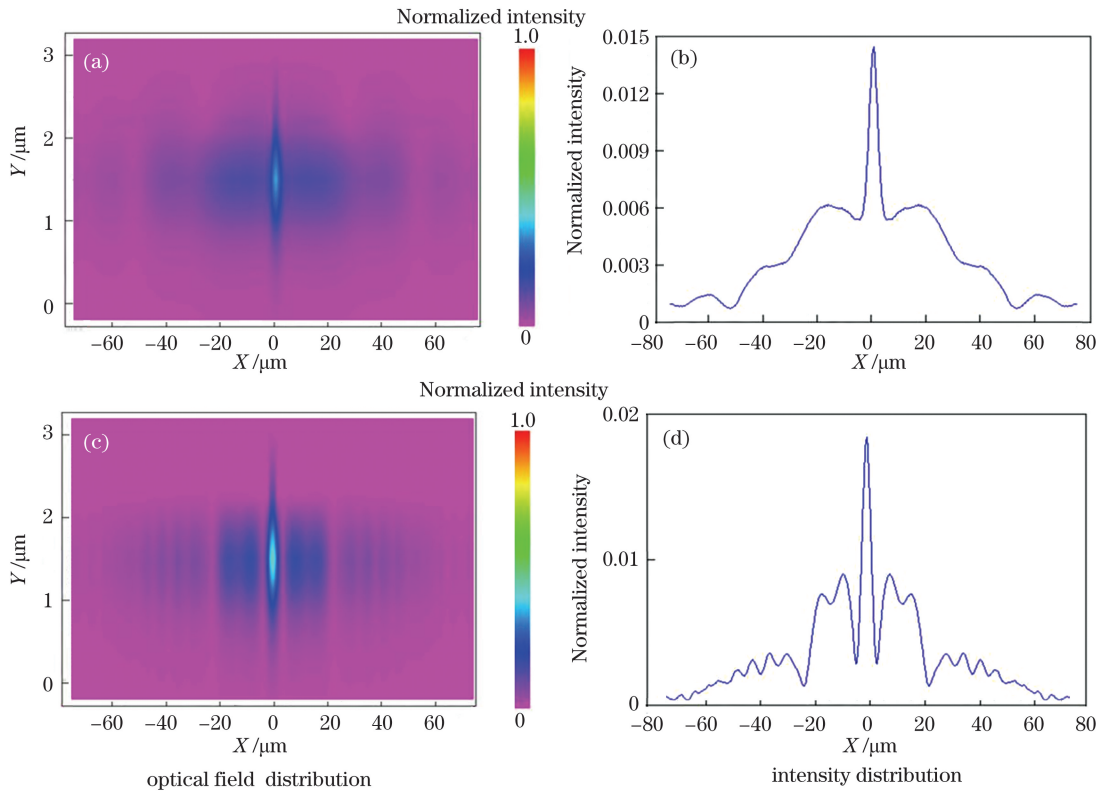


图 2 两种导波模式下后腔面的前向光场分布及其对应的强度分布。(a)(b)增益波导;(c)(d)折射率波导
 Fig. 2 Front-facing optical field distributions of back cavity surfaces for two guided wave modes as well as their corresponding intensity distributions. (a) (b) Gain waveguide; (c) (d) refractive index waveguide

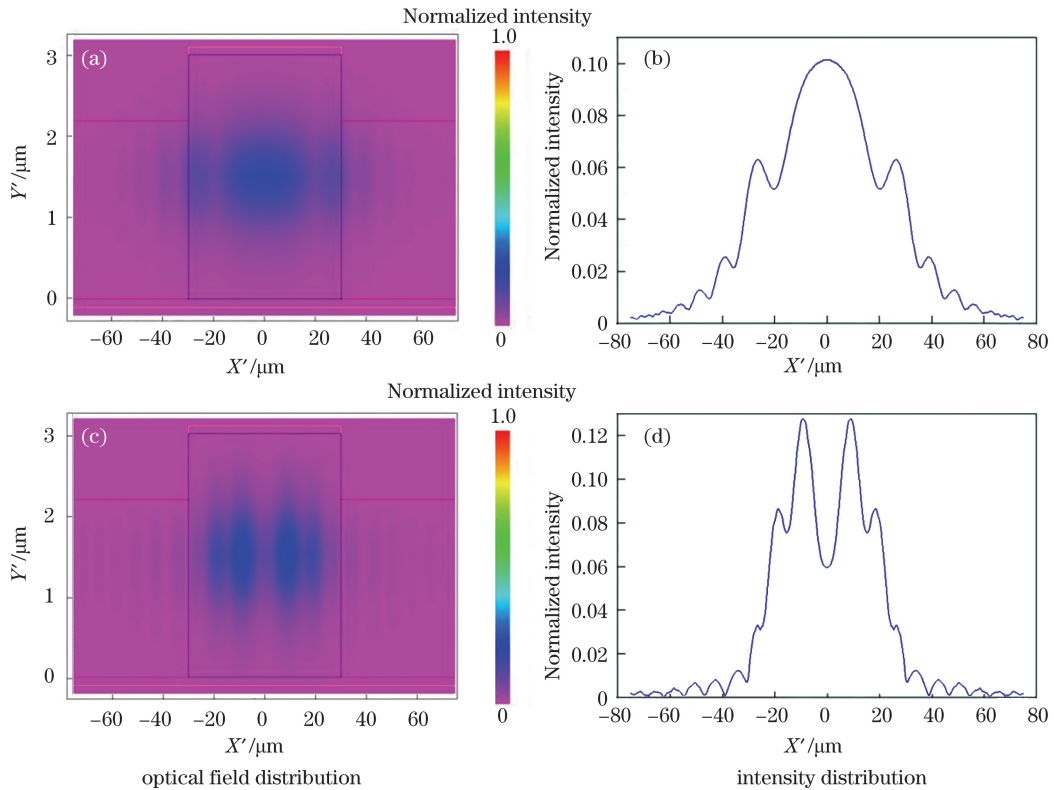


图 3 两种导波模式下前腔面的光场分布及其对应的强度分布。(a)(b)增益波导;(c)(d)折射率波导
 Fig. 3 Optical field distributions of front cavity surfaces for two guided wave modes as well as their corresponding intensity distributions. (a) (b) Gain waveguide; (c) (d) refractive index waveguide

激光器出光面上的光场分布比较均匀,没有强度较高的尖峰出现;而在折射率波导结构激光器中,出光面上的光场分布出现了两个强度较高的尖峰。这主要是因为相较于增益波导结构,折射率波导结构对光的限制作用强,因此前腔面反射回来的光的绝大部分通过散射传播到后腔面,导致后腔面上光场的分布相对比较杂乱;这些到达后腔面的光的大部分是高阶横向模,在后腔面处被反射,沿着单模区外部向前腔面方向传播,如果其传播角度小于锥形激光器的锥角,则它们会在锥面上发生散射,重新进入锥形激光器,这将会触发空间烧孔(Space Hole Burning, SHB)效应,极高的能量集中会引起腔面上的热点效应,进而导致光束成丝现象^[7],严重时还会导致腔面烧毁,直接损坏器件。

3.2 远场特性

远场是指与激光束束腰位置的距离远大于瑞利(Rayleigh)长度的激光辐射场。激光辐射场是在有源层中产生的,有源层仅仅是激光器芯片的一小部分,因此当激光从有源区出来时,会发生衍射现象。在垂直于PN结的方向上,激光器的有源层很窄,光波的衍射作用较强,发出的光束的衍射角较

大;在平行于PN结的方向上,发光区的宽度远大于光波的波长,光波的衍射作用较弱,因此半导体激光器发出的光通常呈椭圆形。由于半导体激光器波导结构的特点,通常输出光束的发散角很大,需要经过光束整形,因此研究其远场特性具有重要意义。

图4给出的是在1.55 V电压条件下,两种导波模式下锥形半导体激光器的远场分布及其对应的强度分布,其中 α_1 、 α_2 分别为激光器水平、垂直方向的远场发散角。增益波导结构的远场发散角约为 $2^\circ \times 40^\circ$ (慢轴远场发散角 \times 快轴远场发散角),折射率波导结构的远场发散角约为 $8^\circ \times 40^\circ$ 。在平行于PN结方向上,折射率波导结构激光器的远场发散角大于增益波导结构的远场发散角,且角度比较小;同时,增益波导结构激光器的远场只有一个光斑,而折射率波导结构激光器的远场出现了两个近乎相同的光斑,这对激光器的应用是极为不利的。在垂直于PN结方向上,两种导波模式下激光器的远场发散角相同,但角度较大。为了降低垂直方向上的远场发散角,可以采用大光腔结构^[19]或光子晶体结构^[20]等。

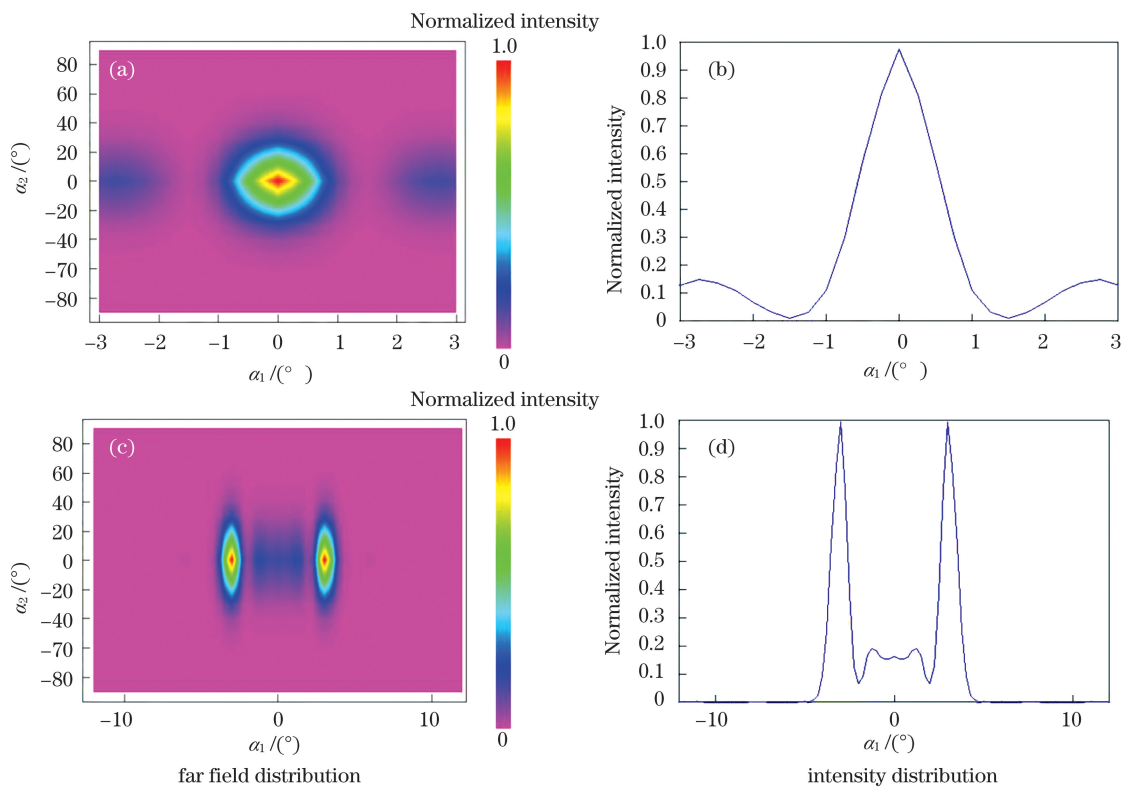


图4 两种导波模式下的远场分布及其对应的强度分布。(a)(b)增益波导;(c)(d)折射率波导

Fig. 4 Far field distributions for two guided wave modes as well as their corresponding intensity distributions.

(a) (b) Gain waveguide; (c) (d) refractive index waveguide

通过模拟计算可以得出,在 1.55 V 电压条件下,折射率波导结构和增益波导结构激光器的光束质量因子分别为 3.9 和 2.5。两种不同导波模式下实际测量的光束质量因子随输出功率的变化情况如图 5 所示。可以看出,在 0~1.5 W 范围内,当输出功率一定时,相较于折射率波导结构,增益波导结构锥形激光器的光束质量因子小,表明其光束特性较好,这进一步验证了模拟结果的准确性。

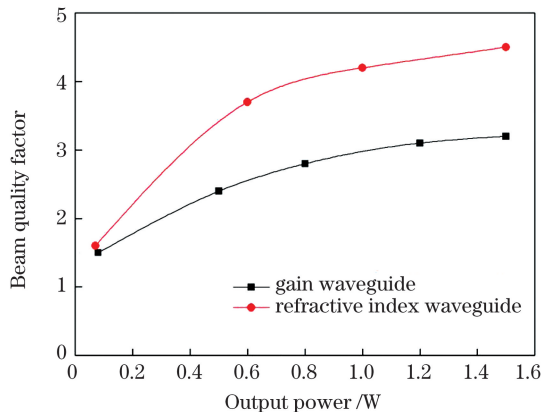


图 5 不同导波模式下光束质量因子

Fig. 5 Beam quality factors for different guided wave modes

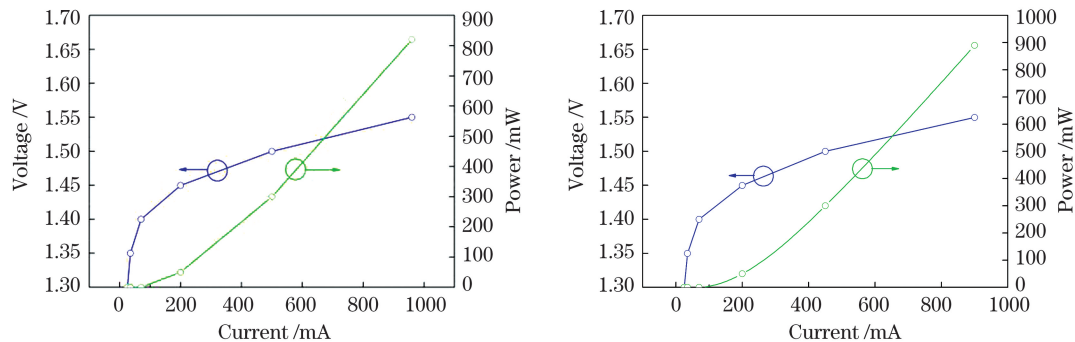


图 6 两种导波模式下的 P-I-V 曲线。(a)增益波导;(b)折射率波导

Fig. 6 P-I-V curves for two guided wave modes. (a) Gain waveguide; (b) refractive index waveguide

4 结 论

采用光波导仿真软件 Rsoft,对比分析了增益波导结构和折射率波导结构对锥形半导体激光器输出特性的影响。结果表明,相对于折射率波导结构,增益波导结构锥形激光器的输出功率虽相对较低,但其输出光束特性较好,这对半导体激光器的应用至关重要。

参 考 文 献

[1] Bachmann F. Industrial applications of high power diode lasers in materials processing [J]. Applied Surface Science, 2003, 208/209: 125-136.
[2] Bachmann F, Loosen P, Poprawe R. High power

3.3 功率-电流-电压特性

图 6 给出的是两种导波模式下锥形半导体激光器的功率-电流-电压 (P-I-V) 特性曲线图,其中图 6(a)为增益波导,图 6(b)为折射率波导。可以看出,在 1.55 V 电压下,增益波导结构锥形激光器的输出光功率为 820 mW,折射率波导结构锥形激光器的输出光功率为 890 mW,两者的输出光功率相差 70 mW。同时,通过计算可知,增益波导结构锥形激光器和折射率波导结构锥形激光器的斜率效率分别为 0.932 W/A 和 1.07 W/A。这是因为相较于增益波导结构,折射率波导结构对光的限制作用强,锥形激光器前腔面反射回来的光限制在单模区两侧而不能被耗散掉,进而从后腔面反射回来并再一次进入锥形区进行放大,因此其输出光功率较高;而在增益波导结构中,其对光的限制作用弱,前腔面反射回来的光有一大部分被损耗掉,不能再次进入锥形区进行光放大,因此其输出光功率相对较低。综合 3.1 节和 3.2 节可以看出,增益波导结构锥形激光器的输出光功率虽然相对较低,但其近远场光束特性较好,这对激光器的应用至关重要。

diode lasers[M]. New York: Springer, 2007.

[3] Vorontsov M A, Weyrauch T. High-power lasers for directed-energy applications: comment [J]. Applied Optics, 2016, 55(35): 9950-9953.
[4] Wang S L, Fang F Z. High power laser and its development [J]. Laser & Optoelectronics Progress, 2017, 54(9): 090005.
王狮凌, 房丰洲. 大功率激光器及其发展 [J]. 激光与光电子学进展, 2017, 54(9): 090005.
[5] Chen L H, Yang G W, Liu Y X. Development of semiconductor lasers [J]. Chinese Journal of Lasers, 2020, 47(5): 0500001.
陈良惠, 杨国文, 刘育衡. 半导体激光器研究进展 [J]. 中国激光, 2020, 47(5): 0500001.
[6] Yuan Q H, Jing H Q, Zhang Q Y, et al.

- Development and applications of GaAs-based near-infrared high power semiconductor lasers [J]. *Laser & Optoelectronics Progress*, 2019, 56(4): 040003.
- 袁庆贺, 井红旗, 张秋月, 等. 砷化镓基近红外大功率半导体激光器的发展及应用 [J]. *激光与光电子学进展*, 2019, 56(4): 040003.
- [7] Dittmar F, Sumpf B, Fricke J, et al. High-power 808-nm tapered diode lasers with nearly diffraction-limited beam quality of $M^2 = 1.9$ at $P = 4.4$ W [J]. *IEEE Photonics Technology Letters*, 2006, 18(4): 601-603.
- [8] Fiebig C, Blume G, Kaspari C, et al. 12 W high-brightness single-frequency DBR tapered diode laser [J]. *Electronics Letters*, 2008, 44(21): 1253-1255.
- [9] Müller A, Fricke J, Bugge F, et al. DBR tapered diode laser with 12.7 W output power and nearly diffraction-limited, narrowband emission at 1030 nm [J]. *Applied Physics B*, 2016, 122(4): 1-6.
- [10] Müller A, Zink C, Fricke J, et al. 1030 nm DBR tapered diode laser with up to 16 W of optical output power [J]. *Proceedings of SPIE*, 2017, 10123: 101231B.
- [11] Pedrola G L. Beam propagation method for design of optical waveguide devices [M]. Chichester: John Wiley & Sons, 2015.
- [12] Scarmozzino R, Gopinath A, Pregla R, et al. Numerical techniques for modeling guided-wave photonic devices [J]. *IEEE Journal of Selected Topics in Quantum Electronics*, 2000, 6(1): 150-162.
- [13] Romero B, Arias J, Esquivias I, et al. Simple model for calculating the ratio of the carrier capture and escape times in quantum-well lasers [J]. *Applied Physics Letters*, 2000, 76(12): 1504-1506.
- [14] Borruel L, Sujecki S, Esquivias I, et al. Self-consistent electrical, thermal, and optical model of high-brightness tapered lasers [J]. *Proceedings of SPIE*, 2002, 4646: 355-366.
- [15] Wenzel H, Erbert G, Enders P M. Improved theory of the refractive-index change in quantum-well lasers [J]. *IEEE Journal of Selected Topics in Quantum Electronics*, 1999, 5(3): 637-642.
- [16] Guo C Z. Semiconductor laser mode theory [M]. Beijing: Posts & Telecom Press, 1989.
- 郭长志. 半导体激光模式理论 [M]. 北京: 人民邮电出版社, 1989.
- [17] Borruel L, Odriozola H, Tijero J M G, et al. Design strategies to increase the brightness of gain guided tapered lasers [J]. *Optical and Quantum Electronics*, 2008, 40(2/3/4): 175-189.
- [18] Li J, Qiu Y T, Cao Y H, et al. Numerical simulation of filamentation induced by waveguide in semiconductor taper amplifiers [J]. *Optik*, 2019, 176: 711-715.
- [19] Ma X L, Qu H W, Zhao S Y, et al. Improved power and efficiency for tapered lasers with optimized photonic crystal structures [J]. *Proceedings of SPIE*, 2017, 10457: 104571O.
- [20] Zhao S Y, Qi A Y, Wang M J, et al. High-power high-brightness 980 nm lasers with $>50\%$ wall-plug efficiency based on asymmetric super large optical cavity [J]. *Optics Express*, 2018, 26(3): 3518-3526.

Influence of Guided Wave Mode on Output Characteristics of Tapered Diode Laser

Yuan Qinghe^{2,3}, Jing Hongqi^{2*}, Liu Suping², Ma Xiaoyu^{2,3}, Ma Xiaohui¹

¹Key Laboratory of High Power Semiconductor Laser for National Defense Technology, Changchun University of Science and Technology, Changchun, Jilin 130022, China;

²National Engineering Research Center for Optoelectronic Devices, Institute of Semiconductors, Chinese Academy of Sciences, Beijing 100083, China;

³College of Materials Science and Optoelectronics, University of Chinese Academy of Sciences, Beijing 100049, China

Abstract

Objective The high power and high beam quality of tapered semiconductor laser output have led to a recent increase in research conducted in this field. Two guided wave modes are mainly used in semiconductor lasers: refractive index and gain waveguides. Little attention is paid to the gain waveguide owing to its unstable mode; instead, refractive index waveguide structures are often used in tapered semiconductor lasers. Although a tapered semiconductor laser with a refractive index waveguide structure can output high power and high beam quality, the product is similar to that of a high-power wide-contact semiconductor laser. The beam is unstable at high power output and is prone to

twisting and causing filamentation. This phenomenon occurs for two reasons. The first is that mode filtering is not ideal in the ridge waveguide part, and the beam injected into the tapered area is not the fundamental mode. The second is that the refractive index changes in the tapered amplification area owing to thermal induction or spatial hole burning, which causes the beam to self-focus. In present studies, the difference in the output characteristics of the gain and refractive index waveguide structures for a tapered semiconductor laser is analyzed. Although the output power of a laser with a gain waveguide structure shows a slight decrease, its beam quality is significantly improved. This study provides a reference for the design of tapered semiconductor lasers with high power and high beam quality.

Methods In this study, the professional optical waveguide simulation software, RSoft, was used to compare and analyze the influences of the gain and refractive index waveguide structures on the output characteristics of a tapered semiconductor laser. First, the structural parameters of a tapered semiconductor laser including the length and width of the single-mode region as well as the length and angle of the tapered region were determined through the relevant theoretical analysis. Then, RSoft was applied to the model for simulation. The near- and far-field distributions, beam quality factor and power-current-voltage characteristics under different guided wave modes were finally determined. In addition, to verify the accuracy of the simulation results, tapered semiconductor lasers with gain and refractive index waveguide structures were fabricated separately, and the beam quality factor was measured using the knife-edge method.

Results and Discussions In the analysis of the near-field distribution, the optical field distribution on the back cavity surface of the gain waveguide structure laser was relatively smooth with no high spikes. In contrast, that of the refractive index waveguide structure laser was relatively rough, with numerous small spikes appearing in the single-mode region (Fig. 2). Furthermore, the optical field distribution on the light-emitting surface of the gain waveguide structure laser was relatively uniform with no high-intensity spikes; that of the laser with a refractive index waveguide structure, however, showed two high-intensity spikes (Fig. 3). The far-field characteristic analysis showed a far-field divergence angle of about $2^\circ \times 40^\circ$ (slow axis \times fast axis) in the gain waveguide structure, and for the refractive index waveguide structure, the angle was about $8^\circ \times 40^\circ$. The far-field divergence angle of the refractive index waveguide structure laser in the direction parallel to the PN junction was larger than that of the gain waveguide structure laser, and the angle was relatively small. The far-field of the gain waveguide structure laser showed only one spot, whereas that of the refractive index waveguide structure laser exhibited two nearly identical spots (Fig. 4). In addition, the beam quality factor of our fabricated device was measured (Fig. 5). In the range of 0–1.5 W, the beam quality factor of the tapered laser with a gain waveguide structure was smaller than that with a refractive index waveguide structure when the output power was constant. Furthermore, the power-current-voltage analysis result indicated that under a voltage of 1.55 V, the output optical power of the tapered laser with a gain waveguide structure was 820 mW, whereas that with a refractive index waveguide structure was 890 mW. Therefore, the output optical power difference between these two lasers was 70 mW (Fig. 6). The slope efficiencies of the gain and refractive index waveguide structures were calculated to be 0.932 W/A and 1.07 W/A, respectively.

Conclusions In this study, the influences of the gain and refractive index waveguide structures on the output characteristics of a tapered semiconductor laser are studied by simulation and experimentation. The results show that under the same voltage condition, the output power of the tapered laser with a gain waveguide structure is relatively lower than that with a refractive index waveguide structure. However, the light field distribution on the output facet is more uniform. The lower output power can effectively reduce the spatial hole burning effects and result in a better far-field distribution. The light confinement effect is stronger in the refractive index waveguide structure than that in the gain waveguide structure, which causes light reflected from the front cavity surface of the tapered laser to be limited to both sides of the single-mode region and prevents dissipation. The light reflected back again enters the tapered area for amplification, resulting in optical power with relatively high output. In the gain waveguide structure, however, the weak light confinement effect causes a large part of the light reflected from the front cavity surface to be lost. Because the light does not re-enter the tapered area for optical amplification, its output optical power is relatively low. Moreover, the strong confinement effect of the refractive index waveguide structure on the light causes most of the light reflected from the front cavity surface to propagate along the back cavity surface through scattering. This in turn causes a relatively messy distribution of the optical field on the back cavity surface. The light reaching the back cavity surface, which is a high-order transverse mode, is reflected from the back cavity

surface and propagates along the front cavity surface outside the single-mode area. If its propagation angle is smaller than the tapered angle of the tapered laser, part of the light will likely re-enter the tapered part to strongly affect the beam quality of the device.

Key words lasers; tapered lasers; gain waveguide; refractive index waveguide; Rsoft; simulation

OCIS codes 140.2020;140.3070;140.3290;140.3295